

# Comparison of the Optical and Electrochemical Properties of Bi(perylene diimide)s Linked through Ortho and Bay Positions

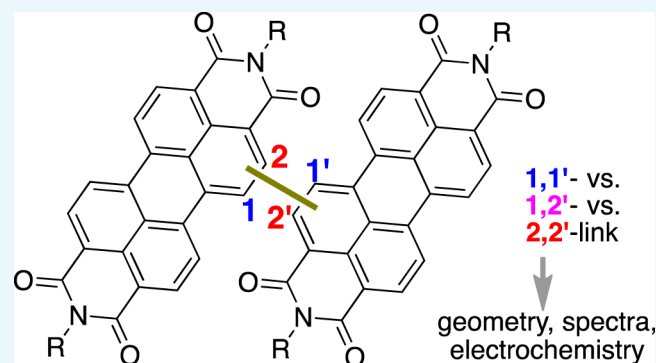
Yeli Fan,<sup>†,‡</sup> Kostiantyn Ziabrev,<sup>‡,§</sup> Siyuan Zhang,<sup>‡,||</sup> Baoping Lin,<sup>†</sup> Stephen Barlow,<sup>‡</sup> and Seth R. Marder<sup>\*,‡,§</sup>

<sup>†</sup>School of Chemistry and Chemical Engineering, Southeast University, Nanjing, Jiangsu 211189, P. R. China

<sup>‡</sup>Center for Organic Photonics and Electronics and School of Chemistry and Biochemistry, Georgia Institute of Technology, Atlanta, Georgia 30332-0400, United States

**S** Supporting Information

**ABSTRACT:** The Ullmann homocoupling of 2-bromoperylene diimides (PDIs) gave [2,2'-biperylene]-3,4:9,10:3',4':9',10'-tetrakis(dicarboximide)s, 2,2'-bi(PDI)s, and the Suzuki coupling of a PDI-2-boronic ester and a 1-bromo-PDI gave a [1,2'-biperylene]-3,4:9,10:3',4':9',10'-tetrakis(dicarboximide), 1,2'-bi(PDI). These were compared with [1,1'-biperylene]-3,4:9,10:3',4':9',10'-tetrakis(dicarboximide)s, 1,1'-bi(PDI)s. Solution absorption spectra suggest that the PDIs in 2,2'-bi(PDI)s are more planar and less strongly coupled than those in 1,1'-bi(PDI)s, which is consistent with density functional theory calculations. 2,2'-Bi(PDI)s are less easily reduced than 1,1'- and 1,2'-bi(PDI)s by ca. 70–90 mV. Bulk heterojunction organic solar cells incorporating a 2,2'-bi(PDI) acceptor behaved similarly to those employing its 1,1'-bi(PDI) analogue.



## INTRODUCTION

Perylene-3,4:9,10-bis(dicarboximide)s (perylene diimides, PDIs) have attracted interest as dyes and pigments, electron-transporting semiconductors in organic field-effect transistors, two-photon-absorbing chromophores, fluorophores, and acceptors in photoinduced electron-transfer reactions for both fundamental studies and optical limiting.<sup>1–4</sup> They have also been extensively used as light-harvesting electron-transporting materials in organic solar cells;<sup>2,3,5</sup> indeed, the first donor–acceptor organic solar cell used a PDI-like acceptor in a bilayer heterojunction with copper phthalocyanine.<sup>6</sup> A wide range of PDI architectures have been used in bulk-heterojunction (BHJ) organic photovoltaics (OPV), including simple small molecules,<sup>7</sup> molecules with bulky 1,7-substituents to hinder aggregation,<sup>8</sup> molecules that form columnar discotic liquid-crystal phases,<sup>9</sup> and conjugated<sup>10</sup> and side-chain<sup>11</sup> polymers. Nonfullerene acceptors for solar cells are still an active subject of research,<sup>12–18</sup> and PDIs remain one of the major classes under investigation.<sup>5</sup> Many of the most efficient examples have three-dimensional (3D) architectures, whereby two or more PDIs are forced out of plane with one another and/or a bridging group.<sup>19</sup> One simple approach to such 3D structures is to directly link two PDIs through their “bay” (1,1') positions (see Figure S1 for the numbering scheme for PDIs), with the PDI units being sterically precluded from achieving coplanarity. A variety of 1,1'-bi(PDI)s, **Ia–j**, have been reported (Figure 1). Delocalization in **Ia**<sup>•–</sup> was investigated,<sup>20</sup> and excitonic coupling and electron/energy transfer were studied in **Ib**,<sup>21</sup>

but most studies focused on BHJ OPV.<sup>22–32a</sup> The precursors are generally 1-bromo-PDIs, which are obtained by electrophilic substitution.<sup>1,3</sup> 2-Functionalized-PDIs have recently become accessible through transition metal catalysis<sup>33–37</sup> and been used to synthesize PDI-bridge-PDI species **V–VII** (Figure 1), whose physical and/or OPV properties have been compared to those of 1-bromo-PDI-derived analogues **II–IV**.<sup>38,39</sup> However, 2,2'-bi(PDI)s have not yet been reported.<sup>b</sup> Here, we report 2,2'-bi(PDI)s (**3a** and **3b**, Scheme 1) and a 1,2'-bi(PDI) (**2a**) and compare their absorption spectra and electrochemistry to those of 1,1'-bi(PDI)s (**1a** and **1b**). We also compare the OPV performance of 2,2'-bi(PDI) **3b** to that of its 1,1'-linked analogue, **1b**.

## RESULTS AND DISCUSSION

Scheme 1 shows the synthesis of **1**, **2**, and **3**. Previously reported **1b** (**Ic**)<sup>22</sup> was made in a similar way to other 1,1'-Bi(PDI)s,<sup>20–22,25,28,29</sup> that is, by the Ullmann homocoupling of **S2b**<sup>22,40</sup> in dimethyl sulfoxide (DMSO) (but with added toluene to improve solubility). Boronic esters (**S3**) were synthesized using the previously described conditions,<sup>35,38,41</sup> and, without purification or characterization, they were treated with CuBr<sub>2</sub> to yield 2-Br-PDIs (**S4**),<sup>37</sup> which were converted to 2,2'-PDIs (**3**) using Ullmann conditions similar to those used

Received: December 21, 2016

Accepted: January 23, 2017

Published: February 3, 2017

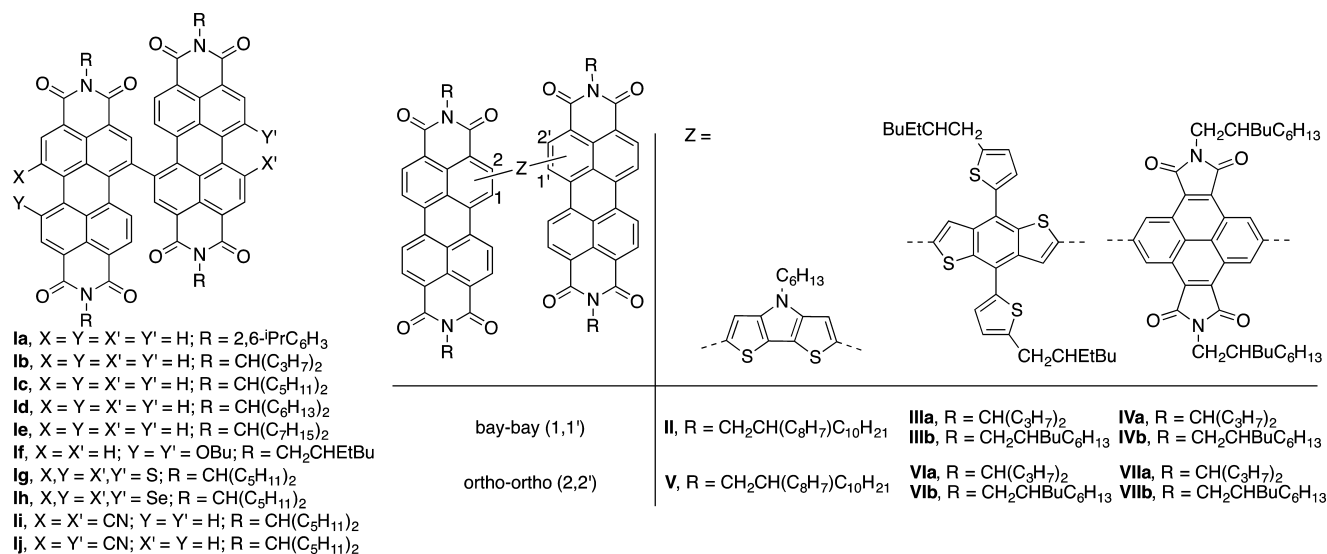


**Figure 1.** Left: reported 1,1'-bi(PDI)s.<sup>22–32</sup> Right: PDI-bridge-PDI species for which comparisons have been made between bay- and ortho-linked species.<sup>38,39</sup>

for 1,1'-PDIs. Boronic ester **S3a** was also subjected to Suzuki coupling conditions with **S2a** to obtain 1,2'-bi(PDI) (**2a**). The new dimers were all characterized by <sup>1</sup>H and <sup>13</sup>C NMR spectroscopy, mass spectrometry, and combustion analysis. Although several of the derivatives show broadened <sup>1</sup>H and/or <sup>13</sup>C spectra, likely as a result of restricted rotation around the PDI–PDI bond, especially in the case of 2,2'-isomers, and about the N-alkyl bonds of the derivatives with CH(C<sub>5</sub>H<sub>11</sub>)<sub>2</sub> chains (as seen for other PDIs with “swallowtail” substituents<sup>42,43</sup>), the isomers can be readily distinguished by NMR (see [Experimental Section](#) and spectra in the [Supporting Information](#)).

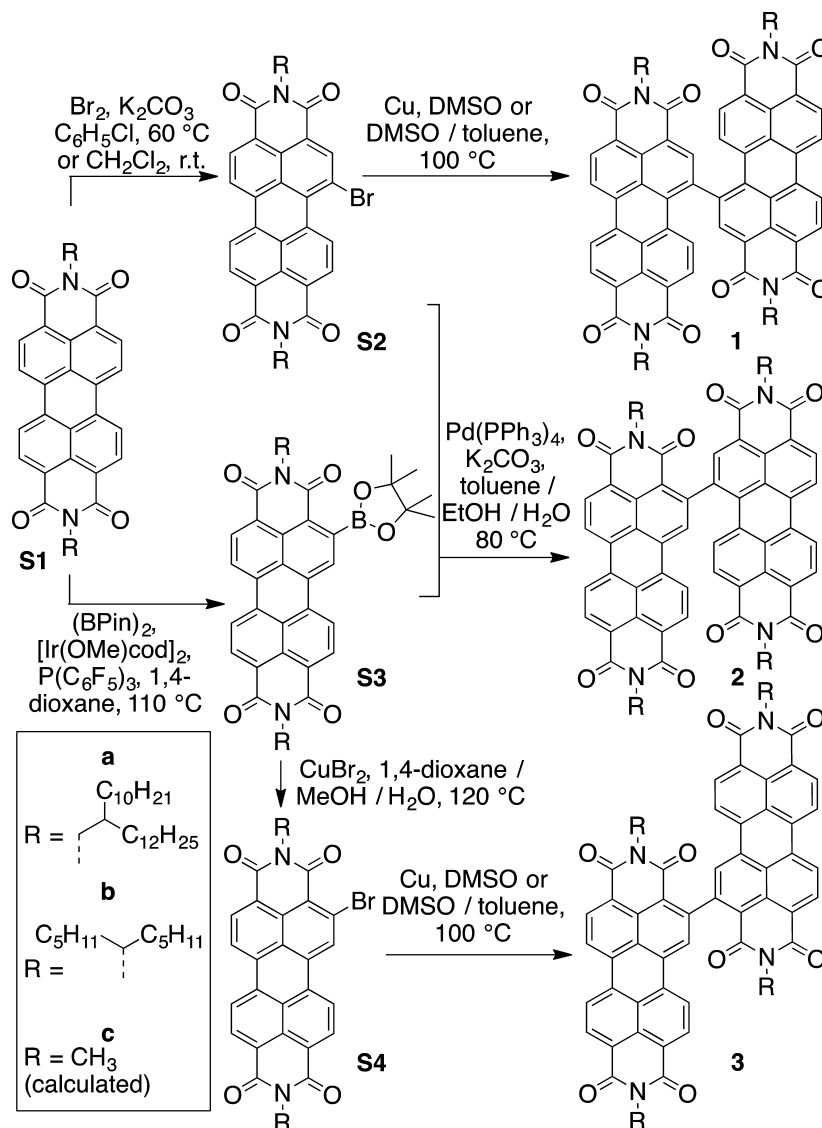
Differential scanning calorimetry (DSC) (10 °C min<sup>-1</sup>, [Figure S2](#)) gave melting points of 167, 188, and 275 °C for **1a**, **2a**, and **3a**, respectively, all considerably higher than that of monomeric **S1a** (108 °C) under the same conditions. In contrast, the bi(PDI)s with secondary alkyl substituents, **1b** and **3b**, showed no evidence of crystallinity, consistent with GIWAXS measurements on **1b**,<sup>30</sup> but exhibited glass transitions at 132 and 85 °C, respectively ([Figure S3](#)). The decomposition temperatures (5 wt % loss, thermogravimetric analysis, 10 °C min<sup>-1</sup>), which vary slightly with linkage motif, are similar to those of monomeric PDIs and are slightly lower for compounds with secondary alkyl imide substituents than for those with branched primary substituents (432, 432, 440, 420, 383, and 381 °C for **1a**, **2a**, **3a**, **S1a**, **1b**, and **3b**, respectively).

Density functional theory (DFT) (B3LYP/6-31G\*\*) calculations for **1c**, **2c**, and **3c** (in which the *N,N'*-dialkyl groups are simplified to CH<sub>3</sub>, [Scheme 1](#)) provide insight into their conformations and energetics. The two PDI units are severely twisted relative to one another, which is consistent with the previous calculations for 1,1'-bi(PDI)s;<sup>20,25,28</sup>  $\psi$ , the CH–C–C–CH torsion angle across the PDI–PDI bond, increases from 1,1'- to 1,2'- and 2,2'-linkages ([Figure 2](#), [Table 1](#)). On the other hand, the two naphthalene subunits of the bay-substituted PDIs of **1c** and **2c** are somewhat twisted from coplanarity (as quantified by  $\phi$ ), whereas the ortho-functionalized PDIs of **2c** and **3c** are virtually planar. Twisted cores are often found for bay-substituted PDIs, even with medium-sized substituents, and they help relieve steric interactions between the 1-substituent and the hydrogen or other substituent in the 12-position.<sup>44–46</sup>

However, steric interaction between 2-substituents and the 3-oxo-group cannot be relieved by an intra-PDI twist,  $\phi$ , and hence results in a larger inter-PDI twist,  $\psi$ . Similar differences in bridge/PDI twists and intra-PDI distortion were seen between bay- and ortho-linked **II** and **V**.<sup>38</sup>

Frontier molecular orbitals for **1c–3c** were also calculated (DFT, B3LYP/6-31\*\*); the wavefunctions and energies for **1c** are similar to those previously reported for **1a**.<sup>20</sup> The LUMO and LUMO + 1 of the symmetric bi(PDI)s (**1c** and **3c**) are bonding and antibonding combinations, respectively, of two PDI LUMOs (see [Table S2](#)). The LUMO/LUMO + 1 energetic separation ([Table 1](#)) is much smaller for **3c** than that for **1c**; this can be attributed to the larger  $\psi$  in **3c**, which reduces the inter-PDI  $\pi$ -overlap, and to the ortho positions of PDIs having smaller LUMO coefficients than the bay positions. Similarly, HOMO and HOMO – 1 resemble, respectively, antibonding and bonding combinations of two PDI HOMOs; again, a larger separation is seen for **1c**. The large LUMO/LUMO + 1 and HOMO/HOMO – 1 separations seen for **2c** are partly due to its inherent asymmetry; the LUMO and HOMO – 1 are localized on the ortho-substituted PDI, whereas the LUMO + 1 and HOMO are localized on the bay-substituted PDI.

[Figure 3](#) compares solution absorption spectra of **1a–3a** and **S1a** ([Figure S4](#) shows spectra of **1b** and **3b**, which are very similar to those of their analogues). Spectra for **1a,b** are consistent with previous reports on 1,1'-bi(PDI)s<sup>20–22</sup> and are considerably broader and more complex than those of monomeric PDIs, such as **S1a**, with lower peak absorptivities ( $\epsilon_{\max}$ ). The broadening and consequent lowering of  $\epsilon_{\max}$  are partially attributed to the nonplanarity of the PDI units,<sup>44,45</sup> however, inter-PDI electronic coupling helps to determine the vibrational structure.<sup>21</sup> Spectra of **3a,b** more closely resemble those of monomeric PDIs, suggesting the PDI units of 2,2'-bi(PDI)s are more planar and less strongly coupled than those of 1,1'-bi(PDI)s, consistent with DFT results (see above). The differences in the linewidth and absorptivity seen here between 1,1'- and 2,2'-PDIs are reminiscent of those previously seen for the PDI-based transitions of **II** and **V**, although the additional complexity attributable to PDI–PDI coupling for **1a,b** is not seen for **II**.<sup>38c</sup> Finally, the spectrum of **2a** is quite similar to that

Scheme 1. Synthesis of 1,1'-, 1,2'-, and 2,2'-bi(PDI)s<sup>a</sup>

<sup>a</sup>Pin = pinacolate; cod = 1,5-cyclooctadiene.

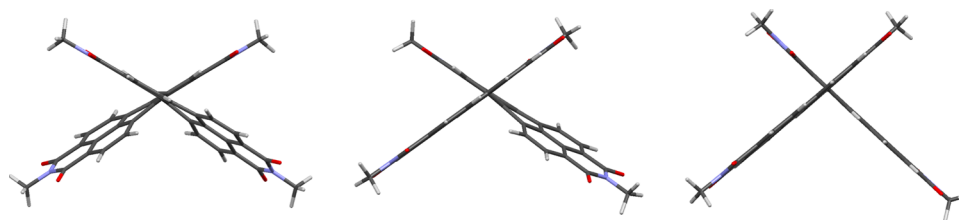


**Figure 2.** Molecular conformations of isolated molecules of, from left to right, 1,1'-, 1,2'-, and 2,2'-Bi(PDI)s (**1c**–**3c**) according to DFT calculations (B3LYP/6-31G\*\*).

of **3a**, but with a lower  $\epsilon_{\max}$  and broadened vibronic sub-bands, consistent with the superposition of the spectra of a planar (ortho-substituted) and less planar (bay-substituted) PDI and with small coupling. Despite a large variation in  $\epsilon_{\max}$ , the oscillator strengths of the main PDI-like bands are similar for all three linkages and only a little less than twice those of **S1a** (Table 2).

PDI–PDI  $\pi$ – $\pi$  interactions typically result in a retained vibronic structure but a decreased ratio of the absorbances of

0,0 to 0,1 sub-bands.<sup>47</sup> Thus, spectra of bi(PDI) thin films (Figure 3) can be understood as resulting from the effects of the planarity and through-bond electronic coupling responsible for the solution spectra and these intermolecular interactions. The variation in  $\pi$ – $\pi$  interactions between bi(PDI)s with different connectivities cannot be easily gauged because of the variation of the solution spectra. However, these effects are more pronounced for the branched primary alkyl derivatives, **1a** and **3a**, than for their secondary alkyl analogues, **1b** and **3b**,

**Table 1. Geometric and Energetic Characteristics of 1,1'-, 1,2'-, and 2,2'-Bi(PDI)s (Isolated Molecules) from DFT Calculations (B3LYP/6-31G\*\*)**

	torsion angles (deg)		orbital energies (eV)			
	$\psi^a$	$\phi^b$	LUMO + 1	LUMO	HOMO	HOMO - 1
1c	70	13	-3.492	-3.659	-6.005	-6.225
2c	70	15, 0 <sup>c</sup>	-3.426	-3.662	-5.927	-6.204
3c	88	0	-3.458	-3.500	-6.025	-6.032

<sup>a</sup>Inter-PDI CH-C-C-CH angle, C2-C1-C1'-C2', C2-C1-C2'-C1', and C1-C2-C2'-C1' for 1c, 2c, and 3c, respectively (see Figure S1 for numbering scheme). <sup>b</sup>Intra-PDI angles C1-C12b-C12a-C6b<sup>1</sup> (Figure S1) quantifying twisting of each PDI core. <sup>c</sup>For 1- and 2-substituted PDIs, respectively.

consistent with the trends for monomeric PDIs<sup>7</sup> and indicating a more disrupted  $\pi$ -stacking when the alkyl branching is immediately adjacent to the nitrogen atoms. The effects of  $\pi$ - $\pi$  interactions appear to be less severe for the bi(PDI)s than for monomeric PDIs (see Figure S4 and spectra of secondary alkyl PDIs in ref 7).

Monomeric PDIs show two successive reversible one-electron reductions. The bi(PDI)s show four solution reductions (Table 2, Figures 3 and S5), consistent with other 1,1'-bi(PDI)s.<sup>20-22,26,28,32</sup> Splittings between redox potentials in compounds with linked equivalent redox centers result from an interplay of effects, including electronic coupling in the mixed-valence species, solvent-mediated Coulombic effects, and through-bond inductive effects.<sup>48</sup> Here, electronic coupling is likely weak: the absorption spectrum of **1a**<sup>•-</sup> indicates that the excess electron is localized on one PDI unit and the coupling is small,<sup>20</sup> and the DFT LUMO/LUMO + 1 splittings (Table 1) suggest an even weaker coupling in 2,2'-bi(PDI)s.<sup>d</sup> For 1,2'-bi(PDI) (**2a**), the inequivalence of the two PDIs may also contribute to the electrochemical splitting.

The first reduction potentials of the bi(PDI)s are similar to one another and to that of **S1a**; however, both the 1,1'- and 1,2'-bi(PDI)s (**1a,b** and **2a**, respectively) are somewhat more readily reduced than the 2,2' dimers (**3a,b**), consistent with the DFT LUMO energies (Table 1), or than **S1a**. The differences between **1a,b** and **3a,b** may be due to the effects of not only planarity but also differences in the inductive and electronic

coupling effects of the linkage motifs. The potential of **2a** is close to that of **1a**, which might suggest its bay-linked PDI that is reduced first; however, DFT indicates that the LUMO of **2a** is localized on the ortho-linked PDI (Table S2), perhaps suggesting that PDI is a more effective inductively electron-withdrawing group through its bay position.

The feasibility of using 2,2'-bi(PDI)s as nonfullerene acceptors in BHJ OPVs was investigated using "inverted" devices with the structure of indium tin oxide (ITO)/ZnO/PTB7-Th:bi(PDI)/MoO<sub>3</sub>/Ag. We compared **1b** and **3b** because (a) **1b** (**1c**) has been used as a nonfullerene acceptor in previous studies<sup>22-24,26,27,30</sup> and (b) monomeric PDIs with secondary alkyl substituents often give more favorable morphologies and better performance than those with linear or branched primary alkyl groups.<sup>7</sup> The device structure and the donor polymer, PTB7-Th (also known as PCE10 and PBDTT-F-TT),<sup>49</sup> were selected on the basis of their previous use with **1b** (**1c**), which gave an optimized power conversion efficiency (PCE) of 5.3% (even higher with a surface modifier applied to ZnO);<sup>24</sup> the same PTB7-Th:**1b** ratio and additives afforded very similar device parameters in our experiment (Table 3, Figure 4). With **3b** as acceptor, the same ratios, additives, and processing gave PCE = 4.8%. However, varying the donor/acceptor ratios and additives led to PCE values close to those for PTB7-Th:**1b** devices (Table 3; see Supporting Information for additional characterization of blends and devices). The similarity in the behavior of the optimized blends is consistent with similar EQE spectra (Figure 4), where, at least for the additive-containing films, the acceptor and donor contributions increase and decrease, respectively, for **3b** versus **1b** films, consistent with a higher acceptor content of the films. The similarity in behavior is also consistent with a fairly small difference in the electron mobility of the blend films ( $5.0 \times 10^{-5}$  and  $2.2 \times 10^{-5}$  cm<sup>2</sup> V<sup>-1</sup> s<sup>-1</sup>, respectively, for the **1b** and **3b** optimized blends; see Figure S8). AFM also suggests similar surface morphologies, although phase images indicate somewhat larger feature sizes for optimized **3b** blends (Figure S7). Overall, at least with PTB7-Th, the 2,2'-bi(PDI) offers no clear advantage over its 1,1' analogue. However, different optimum donor/acceptor/additive compositions found for the two bi(PDI)s indicates they are not interchangeable and suggests that which performs best may vary from system to system.

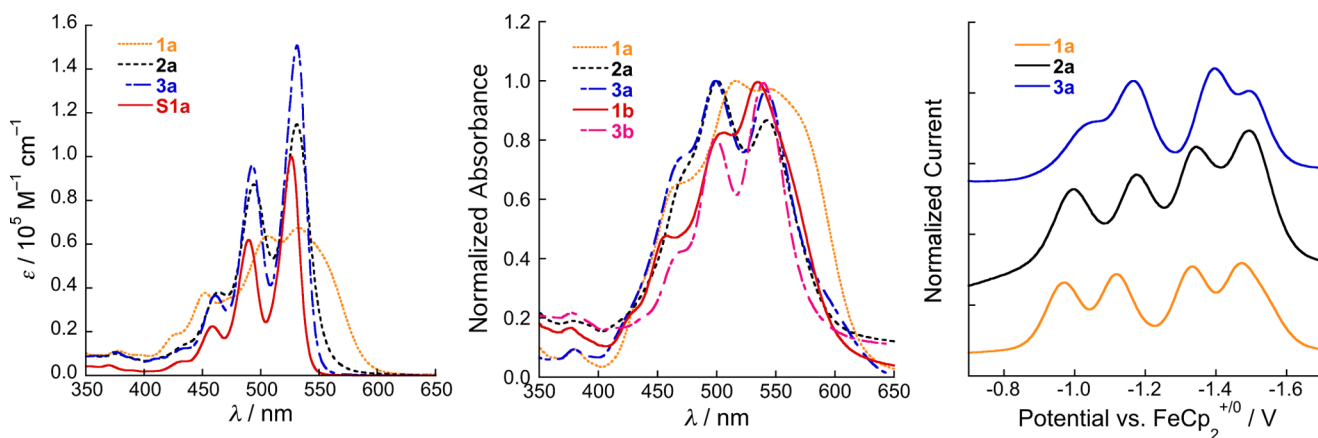


**Figure 3.** Left: Absorption spectra of bi(PDI)s with different linkages and the corresponding monomeric PDI in CHCl<sub>3</sub>. Center: Absorption spectra of films of bi(PDI)s with different linkages and alkyl substituents. Right: Reductive differential pulse voltammograms of bi(PDI)s in THF/0.1 Bu<sub>4</sub>NPF<sub>6</sub>.

Table 2. Electrochemical<sup>a</sup> and Solution Optical Properties<sup>b</sup> of a PDI and 1,1', 1,2', and 2,2'-Bi(PDI)s

	redox potentials versus FeCp <sub>2</sub> <sup>+0</sup> (V)				EA <sub>est</sub> <sup>c</sup> (eV)	λ <sub>max</sub> (nm)	ε <sub>max</sub> (10 <sup>5</sup> M <sup>-1</sup> cm <sup>-1</sup> )	f <sup>d</sup>
	0/-	-/2-	2-/3-	3-/4-				
S1a	-1.07	-1.38			3.7	525	1.0	0.73
1a	-0.97	-1.12	-1.34	-1.48	3.8	532	0.69	1.30
2a	-0.99	-1.18	-1.34	-1.49	3.8	532	1.1	1.27
3a	-1.06	-1.17	-1.40	-1.50	3.7	532	1.5	1.25

<sup>a</sup>Peak reduction potentials from differential pulse voltammetry in tetrahydrofuran (THF)/0.1 M Bu<sub>4</sub>NPF<sub>6</sub>. <sup>b</sup>In chloroform. <sup>c</sup>Estimated solid-state electron affinity obtained from EA = eE<sup>0/-</sup> + 4.8 eV. <sup>d</sup>Oscillator strength obtained as f = 4.32 × 10<sup>-9</sup> ∫ ε dν̄ (ε and ν̄ are in M<sup>-1</sup> cm<sup>-1</sup> and cm<sup>-1</sup>, respectively) over the PDI-like absorption band (ν̄ > 25 000 cm<sup>-1</sup>).

Table 3. Performance of ITO/ZnO/PTB7-Th:biBPI/MoO<sub>3</sub>/Ag Solar Cells<sup>a</sup>

acceptor	D/A wt ratio	additives <sup>b</sup>	V <sub>OC</sub> (V)	J <sub>SC</sub> (mA cm <sup>-2</sup> ) <sup>c</sup>	FF (%)	PCE (%)
1b	1:1		0.74 ± 0.01	12.63 ± 0.35	40.78 ± 1.03	3.81 ± 0.19 (3.99)
1b	1:1	1 wt % DIO + 2 wt % CN	0.76 ± 0.00	12.57 ± 0.29	55.02 ± 0.75	5.24 ± 0.14 (5.44)
3b	1:1.5		0.74 ± 0.01	11.38 ± 0.30	39.85 ± 0.56	3.34 ± 0.15 (3.49)
3b	1:1.5	2 wt % DIO	0.78 ± 0.01	12.57 ± 0.17	52.36 ± 1.07	5.16 ± 0.19 (5.43)

<sup>a</sup>The values are averages from over eight devices; the error bars are standard deviations, and the value of PCE in parentheses is the highest value obtained. <sup>b</sup>DIO = 1,8-diiodooctane; CN = 1-chloronaphthalene.

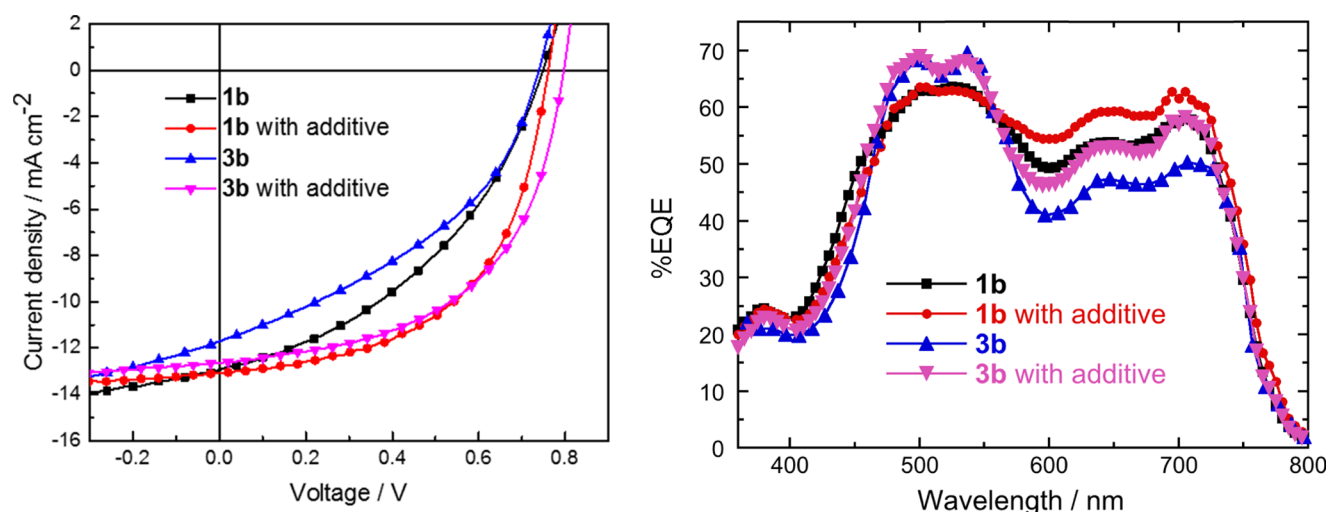


Figure 4. *J*-*V* curves (left) and EQE (right) spectra for ITO/ZnO/PTB7-Th:biBPI/MoO<sub>3</sub>/Ag solar cells (1:1 and 1:1.5 wt ratios for 1b and 3b, respectively) with and without additives (1 wt % DIO + 2 wt % CN for 1b; 2 wt % DIO for 3b).<sup>c</sup> See Figure S6 for the absorption spectra of blend films.

## CONCLUSIONS

1,1', 1,2', and 2,2'-bi(PDI)s differ subtly in their solution absorption spectra and electrochemistry; these changes are consistent with DFT geometries and frontier orbital energies. However, solid-state spectra are more strongly dependent on the nature of the *N,N'*-substituents. A 2,2'-bi(PDI) has been shown to act as a nonfullerene acceptor in BHJ solar cells, and it exhibits a similar performance to its 1,1' analogue, albeit with a different optimum active-layer composition, indicating the 2,2'-bi(PDI) moiety is also a viable building block for nonfullerene acceptors.

## EXPERIMENTAL SECTION

**General Synthesis and Characterization.** Chromatographic separations were performed with standard flash column chromatography methods using silica gel purchased from Sorbent Technologies (60 Å, 40–63 μm). Electrochemical measurements were carried out under nitrogen in dry deoxygenated 0.1 M tetra-*n*-butylammonium hexafluorophos-

phate in THF using a conventional three-electrode cell with a glassy carbon working electrode, a platinum wire counter electrode, and a Ag wire coated with AgCl as the pseudoreference electrode. Potentials were referenced by using ferrocenium/ferrocene as an internal reference. Cyclic voltammograms were recorded at a scan rate of 50 mV s<sup>-1</sup>.

**1-Bromo-*N,N'*-di(2-decyltetradecyl)perylene-3,4:9,10-bis(dicarboximide), S2a.** This compound was previously reported in ref 50 but its synthesis and characterization were not. An alternative preparation involving imidization of a mixture of brominated perylene dianhydrides was reported in ref 51; the characterizing data in ref 51 are consistent with those reported below. *N,N'*-Di(2-decyltetradecyl)perylene-3,4:9,10-bis(dicarboximide), S1a,<sup>52</sup> (6.0 g, 5.6 mmol), K<sub>2</sub>CO<sub>3</sub> (4.0 g, 29 mmol), and chlorobenzene (80 mL) were mixed in a 200 mL round-bottom flask equipped with a condenser. Bromine (4.8 mL, 93 mmol) in chlorobenzene (10 mL) was added dropwise. The reaction mixture was then heated to 60 °C and kept overnight before it was cooled to room

temperature and poured into a saturated  $\text{Na}_2\text{S}_2\text{O}_3$  solution (500 mL). The mixture was extracted with  $\text{CHCl}_3$  ( $2 \times 200$  mL), and the organic phase was washed with water ( $2 \times 100$  mL) and dried over  $\text{Na}_2\text{SO}_4$ . After the solvent was removed, the residue was purified by column chromatography on silica gel, with  $\text{CHCl}_3$ /hexane (1:1) as the eluent. After the solvent was removed under reduced pressure, **S2a** was obtained as a red solid (2.7 g, 42%).  $^1\text{H}$  NMR (500 MHz,  $\text{CDCl}_3$ ):  $\delta$  9.62 (d,  $J = 8.0$  Hz, 1H), 8.72 (s, 1H), 8.51 (m, 3H), 8.36 (m, 2H), 4.09 (d,  $J = 7.0$  Hz, 2H), 4.06 (d,  $J = 7.0$  Hz, 2H), 1.95 (m, 2H), 1.5–1.1 (m, 80H), 0.82 (m, 12H).  $^{13}\text{C}\{^1\text{H}\}$  NMR (125 MHz,  $\text{CDCl}_3$ ):  $\delta$  163.5, 163.2, 163.1, 162.3, 138.9, 133.5, 133.1, 133.0, 130.8, 130.3, 128.5, 128.3, 127.9, 127.6, 126.6, 123.5, 123.4, 123.3, 122.92, 122.7, 122.5, 120.9, 44.79, 44.72, 36.63, 36.58, 31.9, 31.7, 30.1, 30.0, 29.7, 29.6 (2 close peaks), 29.6, 29.4, 26.5 (2 close peaks), 22.7, 14.1 (2 aromatic carbon peaks and 31 alkyl carbon peaks were not observed, presumably due to overlap). HRMS (MALDI-TOF): calcd for  $\text{C}_{72}\text{H}_{103}\text{BrN}_2\text{O}$  ( $\text{M}^+$ ), 1140.728; found, 1140.734. Anal. Calcd for  $\text{C}_{72}\text{H}_{103}\text{BrN}_2\text{O}$ : C, 75.69; H, 9.26; N, 2.45. Found: C, 75.77; H, 9.26; N, 2.50.

***N,N',N'',N'''*-Tetra(2-decyltetradecyl)-[1,1'-biperylene]-3,4:9,10:3',4':9',10'-tetrakis(dicarboximide), 1a.** A mixture of **S2a** (0.25 g, 0.22 mmol), dry toluene (8 mL), and dry DMSO (23 mL) was loaded into a pressure vessel and deoxygenated with a flow of nitrogen; copper powder (40–60 nm particle size, 0.14 g, 2.2 mmol) was then added, and the reaction vessel was sealed and heated to 100 °C for 5 h. The reaction mixture was cooled to room temperature and diluted with dichloromethane (50 mL); the resulting solution was washed with brine and then dried over  $\text{MgSO}_4$ . After filtration and evaporation of the solvents, the crude product was purified by column chromatography (silica gel; 3:2 dichloromethane/hexane), followed by size-exclusion chromatography (SX-1 BioRad; THF) to afford a red solid (0.146 g, 63%). Mp (DSC): 167 °C.  $^1\text{H}$  NMR (500 MHz,  $\text{CDCl}_3$ ):  $\delta$  8.84–8.79 (m, 8H), 8.47 (d,  $J = 8.0$  Hz, 2H), 8.24 (s, 2H), 8.16 (d,  $J = 8.0$  Hz, 2H), 4.08–3.99 (m, 8H), 1.93–1.91 (m, 4H), 1.34–1.17 (m, 160H), 0.87–0.81 (m, 24H).  $^{13}\text{C}\{^1\text{H}\}$  NMR (125 MHz,  $\text{CDCl}_3$ ):  $\delta$  163.85, 163.72, 163.45, 163.36, 142.01, 135.05, 134.49, 134.33, 133.27, 131.92, 131.88, 130.97, 129.53, 129.05, 128.91, 127.81, 127.67, 124.47, 124.28, 123.82, 123.70, 123.65, 123.52, 44.96, 44.84, 36.81, 32.13, 32.09, 31.89, 31.82, 31.80, 31.77, 30.26, 30.22, 30.21, 30.18, 29.90, 29.87, 29.86, 29.84, 29.82, 29.58, 29.56, 29.53, 26.64, 26.46, 22.89, 22.86, 14.32 (1 aromatic carbon peak and 22 alkyl carbon peaks were not observed, presumably due to overlap). HRMS (MALDI-TOF): calcd for  $\text{C}_{144}\text{H}_{211}\text{N}_4\text{O}_8$  ( $\text{MH}^+$ ), 2124.6227; found, 2124.6271. Anal. Calcd for  $\text{C}_{144}\text{H}_{211}\text{N}_4\text{O}_8$ : C, 81.38; H, 9.96; N, 2.64. Found: C, 81.47; H, 10.03; N, 2.66.

**2-(4,4,5,5-Tetramethyl-1,3,2-dioxaborolan-2-yl)-*N,N'*-di(2-decyltetradecyl)perylene-3,4:9,10-bis(dicarboximide), S3a, and 2-Bromo-*N,N'*-di(2-decyltetradecyl)perylene-3,4:9,10-bis(dicarboximide), S4a.** A solution of **S1a**<sup>52</sup> (2.0 g, 1.9 mmol), tris(pentafluorophenyl)phosphine (0.12 g, 0.23 mmol), and bis(pinacolato)diboron (0.57 g, 1.9 mmol) in anhydrous 1,4-dioxane (50 mL) was deoxygenated with argon for 30 min, and then  $(\text{Ir}(\text{OMe})\text{cod})_2$  {cod = 1,5-cyclooctadiene} (0.037 g, 0.056 mmol) was added to a reaction vessel. The resulting mixture was heated to reflux for 24 h, allowed to cool to room temperature, and evaporated under reduced pressure to yield crude **S3a**. For use in the Suzuki coupling with **S2a** to afford **2a**

(see below), the crude product was purified by column chromatography (silica gel; 2:1 to 10:1 dichloromethane/hexane) to afford **S2a** containing minor impurities (0.23 g, 19% yield if pure), which was used in the subsequent Suzuki coupling reactions without additional purification. For conversion to **S4a**, crude **S3a** (1.8 g) (including some unreacted starting material and catalyst) was dissolved in 1,4-dioxane (35 mL); to the resulting red solution, methanol (5 mL) and aqueous  $\text{CuBr}_2$  (1.68 g in 2 mL of water) were added, and the resulting mixture was heated at 120 °C in a sealed tube. After the conversion was complete (ca. 12 h, monitored using thin-layer chromatography (TLC)), the product was extracted with dichloromethane. The extracts were washed with water, dried over  $\text{MgSO}_4$ , filtered, and evaporated under reduced pressure. The resulting residue was purified by column chromatography (silica gel; 3:2 to 5:1 dichloromethane/hexane) to give **S4a** as a red solid (0.626 g, 78% over two steps from **S1a**).  $^1\text{H}$  NMR (500 MHz,  $\text{CDCl}_3$ ):  $\delta$  8.34 (d,  $J = 8$  Hz, 2H), 8.29 (d,  $J = 8$  Hz, 1H), 8.07–8.02 (m, 3H), 7.93 (d,  $J = 8$  Hz, 1H), 4.07 (d,  $J = 7.5$  Hz, 2H), 4.00 (d,  $J = 7.5$  Hz, 2H), 2.05–1.86 (m, 2H), 1.43–1.21 (m, 80H), 0.87–0.83 (m, 12H).  $^{13}\text{C}\{^1\text{H}\}$  NMR (125 MHz,  $\text{CDCl}_3$ ):  $\delta$  162.73, 161.76, 160.60, 132.77, 132.72, 131.59, 130.67, 130.38, 130.16, 129.76, 128.33, 128.12, 124.97, 124.30, 123.17, 122.55, 122.15, 119.86, 44.76, 44.62, 36.60, 36.32, 31.77, 31.75, 31.55, 31.41, 29.98, 29.57, 29.44, 29.22, 29.20, 26.37, 26.23, 22.51 (6  $\text{sp}^2$  and 32 alkyl resonances were not observed, presumably due to overlap). HRMS (MALDI-TOF): calcd for  $\text{C}_{72}\text{H}_{106}\text{BrN}_2\text{O}_4$  ( $\text{MH}^+$ ), 1141.7305; found, 1141.7333. Anal. Calcd for  $\text{C}_{72}\text{H}_{106}\text{BrN}_2\text{O}_4$ : C, 75.69; H, 9.26; N, 2.45. Found: C, 75.80; H, 9.29; N, 2.52.

***N,N',N'',N'''*-Tetra(2-decyltetradecyl)-[1,2'-biperylene]-3,4:9,10:3',4':9',10'-tetrakis(dicarboximide), 2a.** A solution of  $\text{K}_2\text{CO}_3$  (0.087 g, 0.63 mmol) in water (6 mL) was added to a solution of **S3a** (0.32 g, 0.27 mmol) and **S2a** (0.24 g, 0.21 mmol) in a mixture of toluene (60 mL) and EtOH (0.8 mL); after deoxygenation by bubbling with argon for 30 min,  $\text{Pd}(\text{PPh}_3)_4$  (0.026 g, 0.022 mmol) was added, and the resulting mixture was heated to 80 °C under argon overnight. After the conversion of the starting material (according to TLC) was complete, the product was extracted with dichloromethane. The organic phase was washed with water, dried over  $\text{MgSO}_4$ , filtered, and evaporated under reduced pressure. The residue was purified by column chromatography (silica gel; 3:1 dichloromethane/hexane), followed by size-exclusion chromatography (SX-1 BioRad; THF) to give **2a** as a red solid (0.13 g, 29%). Mp (DSC): 188 °C.  $^1\text{H}$  NMR (500 MHz,  $\text{CDCl}_3$ , 325 K):  $\delta$  8.76 (d,  $J = 8.0$ , 1H), 8.71–8.52 (m, 7H), 8.46 (d,  $J = 7.0$ , 1H), 8.41 (s, 1H), 8.37 (d,  $J = 7.0$ , 1H), 8.30–8.20 (m, 1H), 8.02 (d,  $J = 8.5$ , 1H), 7.83 (d,  $J = 8.5$ , 1H), 4.14 (d,  $J = 6.5$ , 2H), 3.96 (d,  $J = 6.5$ , 2H), 3.91–3.60 (m, 4H), 2.03–1.78 (m, 4H), 1.41–1.01 (m, 160H), 0.87–0.78 (m, 24H).  $^{13}\text{C}$  NMR (125 MHz,  $\text{CDCl}_3$ ):  $\delta$  163.79, 163.73, 163.56, 163.40, 163.29, 148.82, 141.25, 135.84, 134.84, 134.66, 134.66, 134.09, 133.39, 131.71, 131.47, 131.09, 130.99, 130.80, 129.43, 129.32, 128.99, 128.27, 127.87, 127.39, 126.24, 125.97, 124.26, 123.96, 123.58, 123.27, 122.90, 122.12, 120.07, 45.08, 44.83, 44.72, 37.01, 36.77, 36.65, 36.43, 32.13, 32.11, 32.10, 31.95, 31.75, 31.70, 31.61, 30.31, 30.27, 30.22, 30.19, 29.90, 29.86, 29.81, 29.75, 29.67, 29.51, 26.76, 26.73, 26.68, 26.58, 26.50, 26.41, 26.34, 22.88, 14.31, 14.30, 14.25 (16  $\text{sp}^2$  and 61 alkyl resonances were not observed, presumably due to overlap). HRMS (MALDI-TOF): calcd for  $\text{C}_{144}\text{H}_{211}\text{N}_4\text{O}_8$  ( $\text{MH}^+$ ), 2124.6227; found,

2124.6300. Anal. Calcd for  $C_{144}H_{210}N_4O_8$ : C, 81.38; H, 9.96; N, 2.64. Found: C, 81.24; H, 9.78; N, 2.74.

***N,N',N'',N'''-Tetra(2-decyltridecyl)-[2,2'-biperylene]-3,4:9,10;3',4':9',10'-tetrakis(dicarboximide), 3a.*** Compound **3a** was synthesized in a similar manner to **1a**, using **S4a** (0.734 g, 0.64 mmol), copper (0.41 g, 6.4 mmol), toluene (17 mL), and DMSO (23 mL), and refluxed overnight to give a red solid (0.232 g, 34%). Mp (DSC): 275 °C.  $^1H$  NMR (500 MHz,  $CDCl_3$ , 325 K):  $\delta$  8.75–8.40 (m, 14H), 4.12–4.04 (m, 4H), 3.92–3.72 (m, 4H), 2.05–1.93 (m, 2H), 1.89–1.78 (m, 2H), 1.41–1.04 (m, 160H), 0.86–0.08 (m, 24H).  $^{13}C\{^1H\}$  NMR (125 MHz,  $CDCl_3$ ):  $\delta$  165.33, 163.69, 163.51, 148.44, 134.36, 134.34, 134.05, 131.63, 130.26, 129.32, 126.30, 123.45, 44.86, 44.41, 36.92, 36.77, 32.13, 32.12, 31.93, 31.71, 30.33, 30.26, 29.91, 29.88, 29.84, 29.77, 29.73, 29.57, 29.55, 29.48, 26.69, 26.38, 22.89, 22.86, 22.83, 14.31, 14.29 (12  $sp^2$  and 23 alkyl resonances were not observed, presumably due to overlap). HRMS (MALDI-TOF): calcd for  $C_{144}H_{210}N_4O_8$  ( $MH^+$ ), 2124.6227; found, 2124.6232. Anal. Calcd for  $C_{144}H_{210}N_4O_8$ : C, 81.38; H, 9.96; N, 2.64. Found: C, 81.54; H, 9.84; N, 2.71.

***N,N',N'',N'''-Tetra(undecan-6-yl)-[1,1'-biperylene]-3,4:9,10;3',4':9',10'-tetrakis(dicarboximide), 1b.*** This compound was synthesized from **S2b**<sup>22,40</sup> according to the literature.<sup>22</sup>  $T_g$  (DSC): 132 °C.  $^1H$  NMR (400 MHz,  $CDCl_3$ ):  $\delta$  8.81–8.77 (m, 8H), 8.49 (d,  $J = 8$  Hz, 2H), 8.19–8.16 (m, 4H), 5.13–5.00 (m, 4H), 2.22–2.14 (m, 8H), 1.80–1.75 (m, 8H), 1.23 (s, 48H), 0.78 (s, 24H).  $^{13}C\{^1H\}$  NMR (100 MHz,  $CDCl_3$ ):  $\delta$  164.70, 164.61, 164.41, 164.32, 164.15, 164.01, 163.68, 163.49, 141.89, 134.23, 131.49, 131.37, 130.62, 130.60, 129.60, 128.86, 128.77, 127.50, 127.38, 124.01, 123.41, 54.94, 54.77, 32.35, 32.30, 31.71, 31.64, 31.62, 26.54, 22.49, 22.47, 13.98 (one aromatic and one alkyl resonance were not observed, presumably due to overlap, whereas the doubling of the carbonyl resonances relative to what is expected for the most symmetric possible conformer is consistent with other studies of PDIs with “swallowtail” substituents and attributable to the effects of restricted rotation about the N–CHR<sub>2</sub> bonds<sup>28</sup>). HRMS (MALDI-TOF): calcd for  $C_{92}H_{106}N_4O_8$  ( $M^+$ ): 1394.8011; found, 1394.8073. Anal. Calcd for  $C_{92}H_{106}N_4O_8$ : C, 79.16; H, 7.65; N, 4.01. Found: C, 78.90; H, 7.68; N, 3.93.

**2-(4,4,5,5-Tetramethyl-1,3,2-dioxaborolan-2-yl)-*N,N'*-di(undecan-6-yl)perylene-3,4:9,10-bis(dicarboximide), S3b, and 2-Bromo-*N,N'*-di(undecan-6-yl)perylene-3,4:9,10-bis(dicarboximide), S4b.** A mixture of **S1b**<sup>53</sup> (2.10 g, 3.00 mmol),  $(Ir(OMe)cod)_2$  (0.06 g, 0.09 mmol), bis(pinacolato)diboron (0.84 g, 3.30 mmol), tris-(pentafluorophenyl)phosphine (0.19 g, 0.36 mmol), and 1,4-dioxane (60 mL) was deoxygenated by bubbling with argon for 30 min. The mixture was then stirred under argon at 110 °C for 24 h. The solvent was removed under reduced pressure after filtering through Celite. The residue (crude **S3b**) was dissolved in dioxane (200 mL), and aqueous  $CuBr_2$  (2.70 g, 12.1 mmol) and methanol (90 mL) were added. The mixture was heated at 120 °C for 12 h. After cooling to room temperature, the mixture was poured into water and extracted with dichloromethane. The organic phase was dried over anhydrous  $Na_2SO_4$ , and the solvent was removed under reduced pressure. The residue was purified by column chromatography (silica gel; 1:1 dichloromethane/hexane) to afford **S4b** as a red solid (0.72 g, 31%).  $^1H$  NMR (400 MHz,  $CDCl_3$ ):  $\delta$  8.73–8.69 (m, 4H), 8.59 (dd,  $J = 4$  Hz, 2H), 8.54 (d,  $J = 8$  Hz, 1H), 5.23–5.16 (m,

2H), 2.29–2.21 (m, 4H), 1.93–1.85 (m, 4H), 1.31–1.24 (m, 24H), 0.86–0.82 (m, 12H).  $^{13}C\{^1H\}$  NMR (100 MHz,  $CDCl_3$ ):  $\delta$  164.47, 163.48, 163.27, 134.55, 134.21, 134.07, 134.03, 132.92, 131.31, 130.70, 129.38, 126.25, 125.63, 123.49, 123.32, 122.91, 55.29, 54.86, 32.23, 32.24, 31.75, 29.71, 26.69, 26.64, 22.57, 14.06 (8  $sp^2$  and 2 alkyl resonances were not observed, presumably due to overlap). HRMS (MALDI-TOF): calcd for  $C_{46}H_{54}N_2O_4Br$  ( $MH^+$ ), 777.3267; found, 777.3239. Anal. Calcd for  $C_{46}H_{53}N_2O_4Br$ : C, 71.03; H, 6.87; N, 3.60. Found: C, 71.10; H, 7.08; N, 3.45.

***N,N',N'',N'''-Tetra(undecan-6-yl)-[2,2'-biperylene]-3,4:9,10;3',4':9',10'-tetrakis(dicarboximide), 3b.*** This compound was synthesized in a similar manner to **1a**, using **S4b** (0.39 g, 0.50 mmol), copper (0.32 g, 5.00 mmol), DMSO (8 mL), and toluene (5 mL), and heated to 100 °C for 5 h. The product was purified by column chromatography (silica gel; 1:1 dichloromethane/hexane) to give a red solid (0.22 g, 64%).  $T_g$  (DSC): 85 °C.  $^1H$  NMR (400 MHz,  $CDCl_3$ ):  $\delta$  8.80–8.71 (m, 8H), 8.56–8.47 (m, 4H), 8.37 (s, 2H), 5.18–4.86 (m, 4H), 2.25–1.74 (m, 16H), 1.27–1.19 (m, 48H), 0.84–0.76 (m, 24H).  $^{13}C\{^1H\}$  NMR (100 MHz,  $CDCl_3$ ):  $\delta$  164.5 (br), 164.4 (br), 163.5 (b), 148.7 (br), 134.52, 134.15, 133.8 (br), 133.6 (br), 132.3 (br), 131.9 (br), 131.6 (br), 131.2 (br), 130.8 (br), 130.53, 129.42, 126.36, 126.13, 124.9 (br), 124.3 (br), 124.0 (br), 123.17, 122.99, 119.31 (br), 54.75, 54.56, 32.31, 32.28, 32.11, 31.73, 31.57, 26.63, 26.54, 22.60, 22.55, 22.45, 14.03, 13.98. HRMS (MALDI-TOF): calcd for  $C_{92}H_{106}N_4O_8$  ( $M^+$ ), 1394.8011; found, 1394.8122. Anal. Calcd for  $C_{92}H_{106}N_4O_8$ : C, 79.16; H, 7.65; N, 4.01. Found: C, 79.28; H, 7.63; N, 3.95.

**Solar-Cell Fabrication and Testing.** ITO-coated glass substrates were ultrasonically cleaned in detergent (sodium dodecyl sulfate), deionized water, acetone, and isopropanol in successive steps. The substrates were treated with UV–ozone for 10 min before use. A thin layer of sol–gel ZnO (ca. 10 nm) was spin-coated onto pre-cleaned ITO-coated glass substrates at 4000 rpm and then annealed at 150 °C for 10 min in air. The ZnO precursor solution was prepared by dissolving  $Zn(OAc)_2 \cdot 2H_2O$  and ethanolamine in 2-methoxyethanol and then stirred overnight. A 24 mg/mL total concentration solution of PTB7-Th and the relevant bi(PDI) in chlorobenzene with different mass ratios and additive concentrations was spin-cast on ZnO layer in a nitrogen-filled glovebox. At the final stage, the substrates were transferred to high vacuum, and  $MoO_3$  (10 nm) topped with silver (100 nm) was thermally evaporated onto the active layer. The active area defined by shadow masks was 0.1  $cm^2$ . The current density–voltage characteristics of the photovoltaic devices were measured in the glovebox using a Keithley 2400 source meter. A xenon arc lamp (300 W) was used as the light source, the intensity of which was calibrated using a KG5-filtered Si cell. The solar-cell performance was measured using an Air Mass 1.5 G solar simulator with an irradiation intensity of 100  $mW/cm^2$ . The thickness of films was measured by a KLA-Tencor P-15 profiler.

**DFT Calculations.** DFT calculations were carried out using the B3LYP functional,<sup>54</sup> which combines Becke's three-parameter hybrid-exchange functional<sup>55</sup> with the Lee–Yang–Parr correlation functional,<sup>56</sup> and the 6-31G\*\* basis set as implemented within the Spartan'14 package.<sup>57</sup> Frequency calculations on the optimized geometries indicated no imaginary frequencies.

## ■ ASSOCIATED CONTENT

### 🔗 Supporting Information

The Supporting Information is available free of charge on the ACS Publications website at DOI: 10.1021/acsomega.6b00537.

PDI atom numbering and definitions of torsion angles; DSC data; additional electrochemical and optical data; additional data characterizing OPV devices and blends; NMR spectra for the bi(PDI)s and new intermediates; additional data and plots from DFT calculations; and Cartesian coordinates for minimized structures (PDF)

## ■ AUTHOR INFORMATION

### Corresponding Author

\*E-mail: seth.marder@chemistry.gatech.edu.

### ORCID

Seth R. Marder: 0000-0001-6921-2536

### Present Addresses

<sup>§</sup>Department of Radiology, Optical Radiology Laboratory, Washington University in St. Louis, School of Medicine, 4515 McKinley Avenue, St. Louis, Missouri 63011, United States (K.Z.).

<sup>||</sup>National Institute of Standards and Technology, 100 Bureau Drive, Gaithersburg, Maryland 20899, United States (S.Z.).

### Notes

The authors declare no competing financial interest.

## ■ ACKNOWLEDGMENTS

This work was supported by the Department of the Navy, Office of Naval Research Award No. N00014-14-1-0580 (CAOP MURI). Y.F. thanks the State-Sponsored Scholarship for Graduate Students from China Scholarship Council. The authors thank Yuting Gao for help with some of the synthetic work and Timothy Parker for help with the DFT calculations.

## ■ ADDITIONAL NOTES

<sup>a</sup>In addition to the compounds shown in Figure 1, halo-substituted derivatives have been reported as precursors to **Ig-i** but have not been studied extensively spectroscopically and electrochemically or in devices.<sup>28,32</sup>

<sup>b</sup>1,1'-Bi(PDI)s have, however, been compared as OPV acceptors with analogues with direct *N,N'*-links.<sup>26,27</sup>

<sup>c</sup>Comparisons between the spectra of **III**, **IV** and **VI**, **VII** are complicated by the effects of aggregation, even in a dilute solution.<sup>39</sup>

<sup>d</sup>Electronic coupling (*V*) in a localized mixed-valence monoanion is given by

$$2V = E_{\text{LUMO}+1} - E_{\text{LUMO}}$$

where the orbital energies refer to the corresponding neutral species, assuming (i) Koopmans' theorem and (ii) that the neutral geometry is a good approximation to that of the monoanion at the symmetric transition state, which connects the two unsymmetrical minima.

<sup>e</sup>Expected  $J_{\text{SC}}$  values obtained from convolution of the four EQE spectra shown in Figure 4 with the AM1.5 spectrum are 12.4, 13.1, 11.4, and 12.4 mA cm<sup>-2</sup>, roughly consistent with the values obtained by *J-V* measurements (note that the values given in Table 3 are averages over eight devices).

## ■ REFERENCES

- (1) Würthner, F. Perylene Bisimide Dyes as Versatile Building Blocks for Functional Supramolecular Architectures. *Chem. Commun.* **2004**, 1564–1579.
- (2) Zhan, X.; Facchetti, A.; Barlow, S.; Marks, T. J.; Ratner, M. A.; Wasielewski, M. R.; Marder, S. R. Rylene and Related Diimides for Organic Electronics. *Adv. Mater.* **2011**, *23*, 268–284.
- (3) Huang, C.; Barlow, S.; Marder, S. R. Perylene-3,4,9,10-Tetracarboxylic Acid Diimides: Synthesis, Physical Properties, and Use in Organic Electronics. *J. Org. Chem.* **2011**, *76*, 2386–2407.
- (4) Liu, Z.; Zhang, G.; Cai, Z.; Chen, X.; Luo, H.; Li, Y.; Wang, J.; Zhang, D. New Organic Semiconductors with Imide/Amide-Containing Molecular Systems. *Adv. Mater.* **2014**, *26*, 6965–6977.
- (5) Fernández-Lázaro, F.; Zink-Lorre, N.; Sastre-Santos, Á. Perylenediimides as Non-Fullerene Acceptors in Bulk-Heterojunction Solar Cells (BHJSCs). *J. Mater. Chem. A* **2016**, *4*, 9336–9346.
- (6) Tang, C. W. Two-Layer Organic Photovoltaic Cell. *Appl. Phys. Lett.* **1986**, *48*, 183–185.
- (7) Sun, J.-P.; Hendsbee, A. D.; Dobson, A. J.; Welch, G. C.; Hill, I. G. Perylene Diimide Based All Small-Molecule Organic Solar Cells: Impact of Branched-Alkyl Side Chains on Solubility, Photophysics, Self-Assembly, and Photovoltaic Parameters. *Org. Electron.* **2016**, *35*, 151–157.
- (8) Sharma, G. D.; Balraju, P.; Mikroyannidis, J. A.; Stylianakis, M. M. Bulk Heterojunction Organic Photovoltaic Devices Based on Low Band Gap Small Molecule BTD-TNP and Perylene–Anthracene Diimide. *Sol. Energy Mater. Sol. Cells* **2009**, *93*, 2025–2028.
- (9) Schmidt-Mende, L.; Fechtenkötter, A.; Müllen, K.; Moons, E.; Friend, R. H.; MacKenzie, J. D. Self-Organized Discotic Liquid Crystals for High-Efficiency Organic Photovoltaics. *Science* **2001**, *293*, 1119–1122.
- (10) Zhan, X.; Tan, Z.; Domercq, B.; An, Z.; Zhang, X.; Barlow, S.; Li, Y.; Zhu, D.; Kippelen, B.; Marder, S. R. A High-Mobility Electron-Transport Polymer with Broad Absorption and Its Use in Field-Effect Transistors and All-Polymer Solar Cells. *J. Am. Chem. Soc.* **2007**, *129*, 7246–7247.
- (11) Zhang, Q.; Cirpan, A.; Russell, T. P.; Emrick, T. Donor–Acceptor Poly(Thiophene-Block-Perylene Diimide) Copolymers: Synthesis and Solar Cell Fabrication. *Macromolecules* **2009**, *42*, 1079–1082.
- (12) Lin, Y.; Zhan, X. Non-Fullerene Acceptors for Organic Photovoltaics: An Emerging Horizon. *Mater. Horiz.* **2014**, *1*, 470–488.
- (13) Eftaiha, F. E.; Sun, J.-P.; Hill, I. G.; Welch, G. C. Recent Advances of Non-Fullerene, Small Molecular Acceptors for Solution Processed Bulk Heterojunction Solar Cells. *J. Mater. Chem. A* **2014**, *2*, 1201–1213.
- (14) Nielsen, C. B.; Holliday, S.; Chen, H.-Y.; Cryer, S. J.; McCulloch, I. Non-Fullerene Electron Acceptors for Use in Organic Solar Cells. *Acc. Chem. Res.* **2015**, *48*, 2803–2812.
- (15) Sauv e, G.; Fernando, R. Beyond Fullerenes: Designing Alternative Molecular Electron Acceptors for Solution-Processable Bulk Heterojunction Organic Photovoltaics. *J. Phys. Chem. Lett.* **2015**, *6*, 3770–3780.
- (16) Zhan, C.; Zhang, X.; Yao, J. New Advances in Non-Fullerene Acceptor Based Organic Solar Cells. *RSC Adv.* **2015**, *5*, 93002–93026.
- (17) Zhan, C.; Yao, J. More Than Conformational “Twisting” or “Coplanarity”: Molecular Strategies for Designing High-Efficiency Nonfullerene Organic Solar Cells. *Chem. Mater.* **2016**, *28*, 1948–1964.
- (18) Lin, Y.; Zhan, X. Oligomer Molecules for Efficient Organic Photovoltaics. *Acc. Chem. Res.* **2016**, *49*, 175–183.
- (19) Lin, Y.; Wang, Y.; Wang, J.; Hou, J.; Li, Y.; Zhu, D.; Zhan, X. A Star-Shaped Perylene Diimide Electron Acceptor for High-Performance Organic Solar Cells. *Adv. Mater.* **2014**, *26*, 5137–5142.
- (20) Jiang, W.; Xiao, C.; Hao, L.; Wang, Z.; Ceymann, H.; Lambert, C.; Di Motta, S.; Negri, F. Localization/Delocalization of Charges in Bay-Linked Perylene Bisimides. *Chem. Eur. J.* **2012**, *18*, 6764–6775.
- (21) Horinouchi, H.; Sakai, H.; Araki, Y.; Sakanoue, T.; Takenobu, T.; Wada, T.; Tkachenko, N. V.; Hasobe, T. Controllable Electronic Structures and Photoinduced Processes of Bay-Linked Perylenedi-



- mid Dimer and a Ferrocene-Linked Triad. *Chem. Eur. J.* **2016**, *22*, 9631–9641.
- (22) Jiang, W.; Ye, L.; Li, X.; Xiao, C.; Tan, F.; Zhao, W.; Hou, J.; Wang, Z. Bay-Linked Perylene Bisimides as Promising Non-Fullerene Acceptors for Organic Solar Cells. *Chem. Commun.* **2014**, *50*, 1024–1026.
- (23) Ye, L.; Jiang, W.; Zhao, W.; Zhang, S.; Qian, D.; Wang, Z.; Hou, J. Selecting a Donor Polymer for Realizing Favorable Morphology in Efficient Non-Fullerene Acceptor-Based Solar Cells. *Small* **2014**, *10*, 4658–4663.
- (24) Zang, Y.; Li, C. Z.; Chueh, C. C.; Williams, S. T.; Jiang, W.; Wang, Z. H.; Yu, J. S.; Jen, A. K. Y. Integrated Molecular, Interfacial, and Device Engineering Towards High-Performance Non-Fullerene Based Organic Solar Cells. *Adv. Mater.* **2014**, *26*, 5708–5714.
- (25) Wang, J.; Yao, Y.; Dai, S.; Zhang, X.; Wang, W.; He, Q.; Han, L.; Lin, Y.; Zhan, X. Oligothiophene-Bridged Perylene Diimide Dimers for Fullerene-Free Polymer Solar Cells: Effect of Bridge Length. *J. Mater. Chem. A* **2015**, *3*, 13000–13010.
- (26) Ye, L.; Sun, K.; Jiang, W.; Zhang, S.; Zhao, W.; Yao, H.; Wang, Z.; Hou, J. Enhanced Efficiency in Fullerene-Free Polymer Solar Cell by Incorporating Fine-Designed Donor and Acceptor Materials. *ACS Appl. Mater. Interfaces* **2015**, *7*, 9274–9280.
- (27) Wu, C.-H.; Chueh, C.-C.; Xi, Y.-Y.; Zhong, H.-L.; Gao, G.-P.; Wang, Z.-H.; Pozzo, L. D.; Wen, T.-C.; Jen, A. K.-Y. Influence of Molecular Geometry of Perylene Diimide Dimers and Polymers on Bulk Heterojunction Morphology toward High-Performance Non-Fullerene Polymer Solar Cells. *Adv. Funct. Mater.* **2015**, *25*, 5326–5332.
- (28) Sun, D.; Meng, D.; Cai, Y.; Fan, B.; Li, Y.; Jiang, W.; Huo, L.; Sun, Y.; Wang, Z. Non-Fullerene-Acceptor-Based Bulk-Heterojunction Organic Solar Cells with Efficiency over 7%. *J. Am. Chem. Soc.* **2015**, *137*, 11156–11162.
- (29) Zhao, J.; Li, Y.; Lin, H.; Liu, Y.; Jiang, K.; Mu, C.; Ma, T.; Lai, J. Y. L.; Hu, H.; Yu, D.; Yan, H. High-Efficiency Non-Fullerene Organic Solar Cells Enabled by a Difluorobenzothiadiazole-Based Donor Polymer Combined with a Properly Matched Small Molecule Acceptor. *Energy Environ. Sci.* **2015**, *8*, 520–525.
- (30) Feng, G.; Xu, Y.; Zhang, J.; Wang, Z.; Zhou, Y.; Li, Y.; Wei, Z.; Li, C.; Li, W. All-Small-Molecule Organic Solar Cells Based on an Electron Donor Incorporating Binary Electron Deficient Units. *J. Mater. Chem. A* **2016**, *4*, 6056–6063.
- (31) Meng, D.; Sun, D.; Zhong, C.; Liu, T.; Fan, B.; Huo, L.; Li, Y.; Jiang, W.; Choi, H.; Kim, T.; Kim, J. Y.; Sun, Y.; Wang, Z.; Heeger, A. J. High-Performance Solution-Processed Non-Fullerene Organic Solar Cells Based on Selenophene-Containing Perylene Bisimide Acceptor. *J. Am. Chem. Soc.* **2016**, *138*, 375–380.
- (32) Yu, Y.; Yang, F.; Ji, Y.; Wu, Y.; Zhang, A.; Li, C.; Li, W. A Perylene Bisimide Derivative with a LUMO Level of  $-4.56$  eV for Non-Fullerene Solar Cells. *J. Mater. Chem. C* **2016**, *4*, 4134–4137.
- (33) Nakazono, S.; Easwaramoorthi, S.; Kim, D.; Shinokubo, H.; Osuka, A. Synthesis of Arylated Perylene Bisimides through C–H Bond Cleavage under Ruthenium Catalysis. *Org. Lett.* **2009**, *11*, 5426–5429.
- (34) Bullock, J. E.; Vagnini, M. T.; Ramanan, C.; Co, D. T.; Wilson, T. M.; Dicke, J. W.; Marks, T. J.; Wasielewski, M. R. Photophysics and Redox Properties of Rylene Imide and Diimide Dyes Alkylated Ortho to the Imide Groups. *J. Phys. Chem. B* **2010**, *114*, 1794–1802.
- (35) Teraoka, T.; Hiroto, S.; Shinokubo, H. Iridium-Catalyzed Direct Tetraborylation of Perylene Bisimides. *Org. Lett.* **2011**, *13*, 2532–2535.
- (36) Battagliarin, G.; Li, C.; Enkelmann, V.; Müllen, K. 2,5,8,11-Tetraboronic Ester Perylenediimides: A Next Generation Building Block for Dye-Stuff Synthesis. *Org. Lett.* **2011**, *13*, 3012–3015.
- (37) Battagliarin, G.; Zhao, Y.; Li, C.; Müllen, K. Efficient Tuning of Lumo Levels of 2,5,8,11-Substituted Perylenediimides Via Copper Catalyzed Reactions. *Org. Lett.* **2011**, *13*, 3399–3401.
- (38) Zhang, J.; Singh, S.; Hwang, D. K.; Barlow, S.; Kippelen, B.; Marder, S. R. 2-Bromo Perylene Diimide: Synthesis Using C–H Activation and Use in the Synthesis of Bis(Perylene Diimide)-Donor Electron-Transport Materials. *J. Mater. Chem. C* **2013**, *1*, 5093–5100.
- (39) Zhao, D.; Wu, Q.; Cai, Z.; Zheng, T.; Chen, W.; Lu, J.; Yu, L. Electron Acceptors Based on A-Substituted Perylene Diimide (PDI) for Organic Solar Cells. *Chem. Mater.* **2016**, *28*, 1139–1146.
- (40) Schmidt, C. D.; Lang, N.; Jux, N.; Hirsch, A. A Facile Route to Water-Soluble Coronenes and Benzo[ghi]Perylenes. *Chem. Eur. J.* **2011**, *17*, 5289–5299.
- (41) Ito, S.; Hiroto, S.; Shinokubo, H. Synthesis of Pyridine-Fused Perylene Imides with an Amidine Moiety for Hydrogen Bonding. *Org. Lett.* **2013**, *15*, 3110–3113.
- (42) Wescott, L. D.; Mattern, D. L. Donor- $\sigma$ -Acceptor Molecules Incorporating a Nonadecyl-Swallowtailed Perylenediimide Acceptor. *J. Org. Chem.* **2003**, *68*, 10058–10066.
- (43) Huang, C.; Potsavage, W. J.; Tiwari, S. P.; Sutcu, S.; Barlow, S.; Kippelen, B.; Marder, S. R. Polynorbornenes with Pendant Perylene Diimides for Organic Electronic Applications. *Polym. Chem.* **2012**, *3*, 2996–3006.
- (44) Würthner, F.; Stepanenko, V.; Chen, Z.; Saha-Möllner, C. R.; Kocher, N.; Stalke, D. Preparation and Characterization of Regioisomerically Pure 1,7-Disubstituted Perylene Bisimide Dyes. *J. Org. Chem.* **2004**, *69*, 7933–7939.
- (45) Chao, C.-C.; Leung, M.-K.; Su, Y. O.; Chiu, K.-Y.; Lin, T.-H.; Shieh, S.-J.; Lin, S.-C. Photophysical and Electrochemical Properties of 1,7-Diaryl-Substituted Perylene Diimides. *J. Org. Chem.* **2005**, *70*, 4323–4331.
- (46) Schmidt, R.; Oh, J. H.; Sun, Y.-S.; Deppisch, M.; Krause, A.-M.; Radacki, K.; Braunschweig, H.; Könemann, M.; Erk, P.; Bao, Z.; Würthner, F. High-Performance Air-Stable n-Channel Organic Thin Film Transistors Based on Halogenated Perylene Bisimide Semiconductors. *J. Am. Chem. Soc.* **2009**, *131*, 6215–6228.
- (47) Li, A. D. Q.; Wang, W.; Wang, L.-Q. Folding versus Self-Assembling. *Chem. Eur. J.* **2003**, *9*, 4594–4601.
- (48) Winter, R. F. Half-Wave Potential Splittings  $\Delta E_{1/2}$  as a Measure of Electronic Coupling in Mixed-Valent Systems: Triumphs and Defeats. *Organometallics* **2014**, *33*, 4517–4536.
- (49) Liao, S.-H.; Jhuo, H.-J.; Cheng, Y.-S.; Chen, S.-A. Fullerene Derivative-Doped Zinc Oxide Nanofilm as the Cathode of Inverted Polymer Solar Cells with Low-Bandgap Polymer (PTB7-Th) for High Performance. *Adv. Mater.* **2013**, *25*, 4766–4771.
- (50) Shoaee, S.; Clarke, T. M.; Huang, C.; Barlow, S.; Marder, S. R.; Heeney, M.; McCulloch, I.; Durrant, J. R. Acceptor Energy Level Control of Charge Photogeneration in Organic Donor/Acceptor Blends. *J. Am. Chem. Soc.* **2010**, *132*, 12919–12926.
- (51) Zhan, X.; Zhang, J.; Tang, S.; Lin, Y.; Zhao, M.; Yang, J.; Zhang, H.-L.; Peng, Q.; Yu, G.; Li, Z. Pyrene Fused Perylene Diimides: Synthesis, Characterization and Applications in Organic Field-Effect Transistors and Optical Limiting with High Performance. *Chem. Commun.* **2015**, *51*, 7156–7159.
- (52) Odom, S. A.; Kelley, R. F.; Ohira, S.; Ensley, T. R.; Huang, C.; Padilha, L. A.; Webster, S.; Coropceanu, V.; Barlow, S.; Hagan, D. J.; Van Stryland, E. W.; Brédas, J. L.; Anderson, H. L.; Wasielewski, M. R.; Marder, S. R. Photophysical Properties of an Alkyne-Bridged Bis(Zinc Porphyrin)-Perylene Bis(Dicarboximide) Derivative. *J. Phys. Chem. A* **2009**, *113*, 10826–10832.
- (53) Demmig, S.; Langhals, H. Leichtlösliche, Lichtechte Perylen-Fluoreszenzfarbstoffe. *Chem. Ber.* **1988**, *121*, 225–230.
- (54) Stephens, P. J.; Devlin, F. J.; Chabalowski, C. F.; Frisch, M. J. *Ab Initio* Calculation of Vibrational Absorption and Circular Dichroism Spectra Using Density Functional Force Fields. *J. Phys. Chem.* **1994**, *98*, 11623–11627.
- (55) Becke, A. D. Density-Functional Exchange-Energy Approximation with Correct Asymptotic Behavior. *Phys. Rev. A* **1988**, *38*, 3098–3100.
- (56) Lee, C.; Yang, W.; Parr, R. G. Development of the Colle-Salvetti Correlation-Energy Formula into a Functional of the Electron Density. *Phys. Rev. B* **1988**, *37*, 785–789.
- (57) *Spartan'14*; Wavefunction Inc.: Irvine, CA.